Chapter 6

Glass Transition of Ultrathin Sugar Films Probed by X-Ray Reflectivity

Shigesaburo Ogawa and Isao Takahashi

Additional information is available at the end of the chapter

http://dx.doi.org/10.5772/66432

Abstract

Besides being the main types of carbohydrate in food, sugars are a representative protectant in biopharmaceutical formulations. To identify the protection mechanism, researchers have extensively investigated the bulk physicochemical properties of sugars. However, whereas the glass transition of sugar has been widely studied and debated, the physicochemical properties of sugar molecules in confined circumstances such as nanometer thick films remain largely unknown. In this chapter, we introduce an experimental procedure for analyzing the glass transition of sugars in ultrathin films. The analysis is based on X-ray reflectivity (XRR) analysis, which has been often applied in glass transition studies of polymer films, but never in sugar media.

Keywords: sugar, ultrathin film, thickness, X-ray reflectivity

1. Introduction

Amorphous sugars form a glassy matrix under far from equilibrium conditions (i.e., supercooling or supersaturation) [1–3]. For instance, sugar glass is obtained by cooling the sugar melt to temperatures far below the melting point (T_m) [1] or by greatly concentrating the sugar solution (i.e., aqueous sugar solution) by evaporation, or by freezing the solvent [2, 3]. The glassy sugar matrix restricts the mobility of incorporated biological molecules and the diffusion of active chemicals, effectively preventing the aggregation and gelation of the biological molecules. Understanding the features of such "sugar glasses," which are already greatly exploited in the food, biology, biochemistry, and pharmaceutical industries [4–10], is pivotal to further development of those diverse fields. Among the numerous sugar compounds, nonreduced oligosaccharides trehalose (Tre) and sucrose (Suc) are generally accepted as

representative stabilizers of biopharmaceutical materials. The structures of these sugars are depicted in **Figure 1a** and **b**, respectively.

The specific heat and coefficient of expansion of a sugar melt abruptly change across the glass transition [1]. In the glassy state, both values are much closer to the crystalline values than the liquid-state values. The glass transitions of bulk sugar-water mixtures at various concentrations are commonly studied by differential scanning calorimetry (DSC), which detects the glass transition as a change in heat capacity. However, DSC thermograms often contain a problematic overshoot peak caused by a macroscopic dynamic process accompanying structural relaxation at the glass transition, which largely depends on the thermal history of the sample [11]. The temperature dependence of the dynamical behavior of amorphous sugar has been widely studied from a thermodynamic perspective [12].

On the other hand, the preparation dependence of the physical properties of amorphous sugar has also received much attention [13–15]. Surana et al. reported that together with aging, the preparation methods (i.e., freeze-drying, spray-drying, dehydration, and melt quenching) largely affect the glass transition temperature (T_g), the enthalpy relaxation behavior, the crystallization behavior, and the water sorption behavior of amorphous trehalose [13, 14]. They also mentioned that water vapor sorption could remove the structural history effects of the amorphous trehalose matrix formed by the dehydration method. More recently, Saxena et al. reported pronounced differences among the water sorption behaviors of amorphous trehalose prepared by different methods (annealing reversal, water sorption-desorption, and heating above T_g) [15]. These results strongly indicate that the properties of amorphous sugar materials are sensitive to water sorption and desorption. The importance of these findings in the pharmaceutical field cannot be overstated.

Specular X-ray reflectivity (XRR) is a unique and powerful analytical method (**Figure 2**) that is frequently applied to condensed soft-matter films, including glass transition studies of ultrathin polymer films [16–20], but which has not been applied in amorphous sugar studies. XRR can evaluate the layered structure of a material, such as the film thickness, electron density, surface roughness, and interfacial width [21, 22]. When the incident X-ray angle in the $2\theta/\omega$ scan exceeds the total reflection critical angle (θ_C), some of the X-rays penetrate the first layer, while the others reflect from the first-layer surface (**Figure 2a**). In turn, some of the penetrating X-rays enter the second layer, while the others reflect at that layer. The phase difference between the X-rays reflected from the two layers creates an interference pattern. Because the

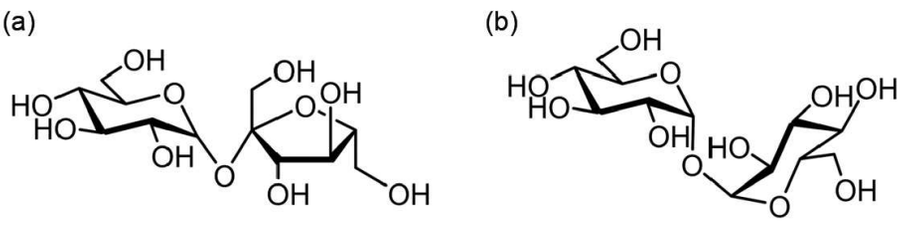

Figure 1. Molecular structures of two natural sugars: sucrose (Suc) (a) and trehalose (Tre) (b).

http://dx.doi.org/10.5772/66432

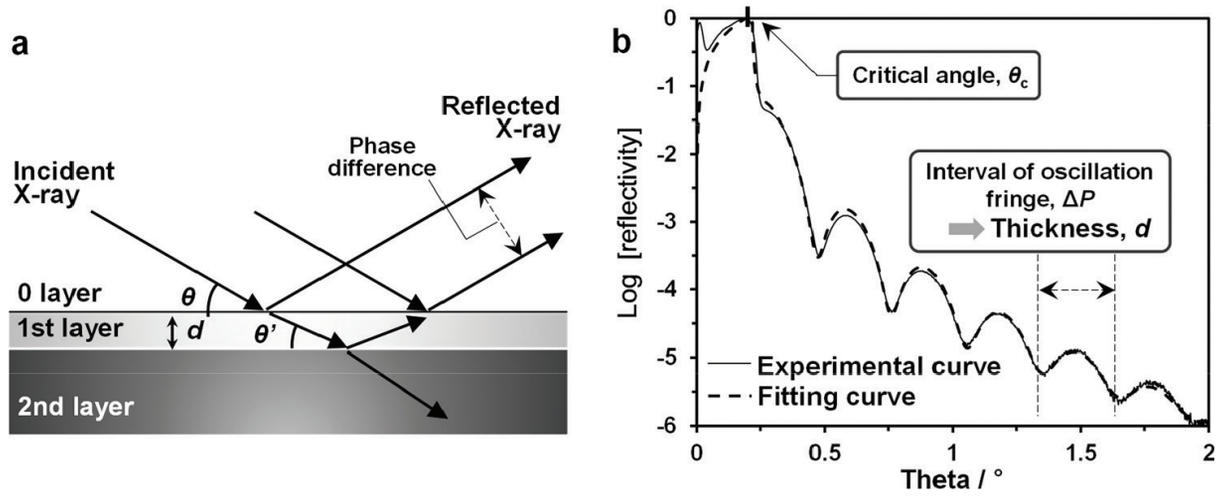

Figure 2. Schematic of XRR analysis (a) and a representative XRR profile, together with a fitting profile calculated by designated software (b).

observed X-ray scattering is the sum of the X-rays reflected by the electrons in each layer, the layers (including the substrate) are easily distinguished by their electron density differences. **Figure 2b** shows representative X-ray profiles of sugar thin film supported on silicon wafer substrate. When the X-ray reflectivity is plotted as a function of incident angle, oscillation fringes caused by X-ray interference appear in the profiles. Oscillation fringes are called "Kiessig fringes" after Kiessig, who first reported them in 1931 [23]. The oscillation period ΔP [radian] heavily depends on the film thickness, d; specifically, d is approximated by $\lambda/(2\Delta P)$, where λ is the X-ray wavelength [21], and is often calculated by fitting the X-ray profiles using an appropriate software [22]. In conventional X-ray optics with multilayer mirrors, this method is highly sensitive to the vertical length scale, which varies from 0.5 to 100 nm. Therefore, it has been extensively used to probe regions close to the interfaces of nano-films and is generally considered unsuitable for bulk material. Importantly, XRR is a nondestructive method, meaning that variations in the structural and morphological parameters of the film can be probed in the same sample. On account of these features, XRR analysis should also become a significant tool for investigating sugar nano-films, but this idea has been insufficiently studied.

The preparation of sugar film has been reported in several articles. Tre and Suc films have been prepared by drop casting [24] or spin coating [25–27] aqueous solutions of the sugar in atmospheric air or by vacuum deposition under reduced pressure [28]. In those reports, the films were thicker than 100 nm. On the other hand, Zhao et al. prepared glucose nano-films with thicknesses ranging from 20 to 60 nm [29]. They studied the adhesion and detachment behaviors of glassy, viscoelastic, and Newtonian liquid states of glucose and characterized the effect of the sugar glassy state on the surface deformations and flows. However, to our knowledge, Tre and Suc nano-films with thicknesses below 100 nm have not been fabricated, and detailed studies of their glass transitions and other properties have not been investigated. We prepared flat nano-films of Tre or Suc sugars by spin coating the aqueous sugar solutions onto silicon wafers and analyzed them by XRR. Large, fairly flat films are required, as the

XRR method has a very small angle of incidence. The effects of the vacuum operation and temperature on the spin-coated films were investigated, and the usefulness of XRR and some novel phenomenon related to the features of sugar glass are disclosed.

2. Experimental

2.1. Materials

Tre dihydrate, Suc, and ultrapure water were purchased from Wako Pure Chemical Co. Ltd. Si(100) substrate (thickness *ca.* 525 μm) was obtained from Electronics and Materials Corp. The Si(100) substrate was cut into a (2 × 2) cm^2 square and washed with ethanol prior to use.

2.2. Preparation of sugar nano-films

Tre and Suc were dissolved in ultrapure water by heating. Sugar nano-films were then prepared by spin coating the aqueous solutions on the Si(100) substrates at 4000 rpm for 45 s.

2.3. X-ray analyses on sugar nano-films

X-ray analyses of the sugar nano-films were performed in a multipurpose X-ray diffractometer (SmartLab, Rigaku Corp., Japan) equipped with a temperature control unit. Prior to measurements, the surface temperature calibration of the Si(100) substrate was checked by a conventional digital multimeter with a thermocouple wire. Specular XRR and X-ray diffraction (XRD) profiles were obtained by $2\theta/\omega$ scanning in the ranges θ = 0–2° and θ = 8–30°, respectively (Cu Kα, wavelength = 0.15418 Å) under air or vacuum conditions. The atmospheric pressure was reduced by a conventional oil hydraulic pump. The thickness and electron density of the films were determined by fitting the XRR profiles in the θ = 0–2° range using a numerical program developed in-house with Origin software. Our software adopted a recursive method based on dynamic scattering theory [30]. Grazing-incidence wide-angle X-ray diffraction (GI-XD) analysis was performed by 2θ scanning over the 2θ = 8–30° range at fixed incident angle (0.2°).

3. Results and discussion

3.1. Estimation of film thickness of spun-films

Figure 3 shows the XRR profile of the Si(100) substrate washed with ethanol. The X-ray reflection intensity was smoothly attenuated and no oscillation fringes were discernible at X-ray incidence angles above θ_C-Si (≈0.22°). This indicates that the surface layer of Si(100) was too thick or too thin for detectable interference between the media of different electron densities by XRR. In fact, the XRR profile fitting of the Si(100) substrate confirmed the absence of any layer thicker than 1 nm, meaning that the single crystal layer of the Si(100) substrate had been thoroughly cleaned. Sugar nano-films of different thicknesses were then prepared by spin coating aqueous sugar solutions of various concentrations onto the cleaned substrates.

http://dx.doi.org/10.5772/66432

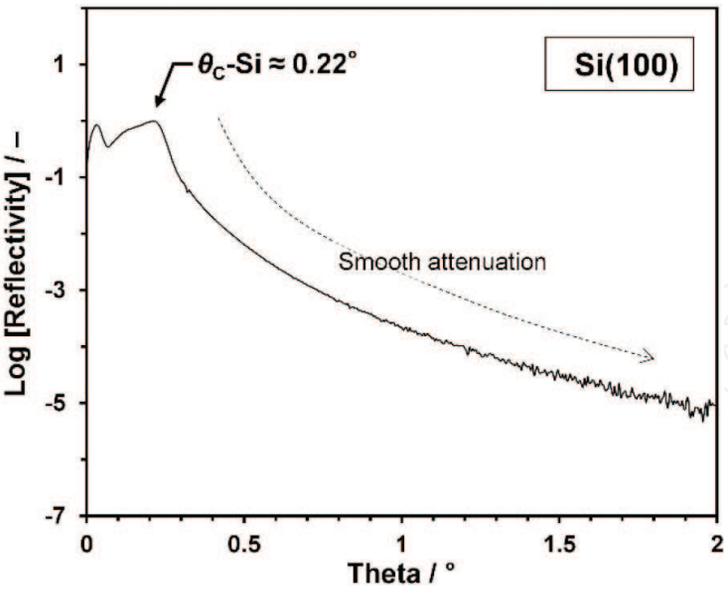

Figure 3. XRR profile of Si(100) substrate after washing with ethanol solvent. θ_c-Si is the critical angle of the Si wafer.

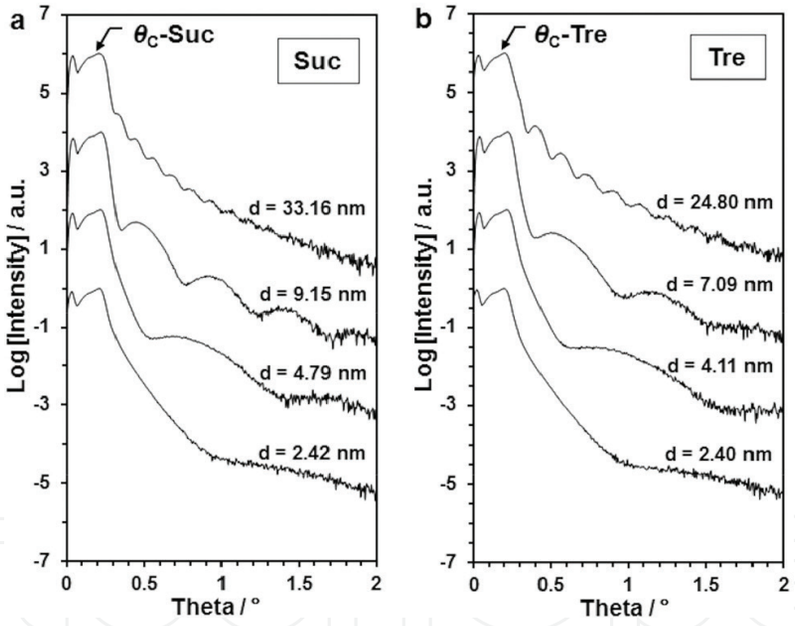

Figure 4. XRR profiles of Suc films (a) and Tre films (b) fabricated at a different thickness, *d*. Each profile represents a sugar film prepared by spin coating. The concentrations of the aqueous sugar solutions were 0.25, 0.50, 1.0, and 3.0 wt% from bottom to top. θ_C-Suc and θ_C-Tre are the critical angles of Suc and Tre films, respectively.

Figure 4 shows an XRR profile series of the spin-coated sugar films. The film thicknesses were calculated by fitting the XRR profiles. Along the series, the film thickness ranged from several to several dozens of nm, and clear oscillation fringes (Kiessig fringes) were observed in θ ranges above the critical incident angle θ_c-Suc and θ_c-Tre of Suc and Tre, respectively. The oscillation period ΔP appears to decrease with increasing concentration of the aqueous solution. As the thickness d is proportional to the reciprocal of ΔP [21], this result implies that

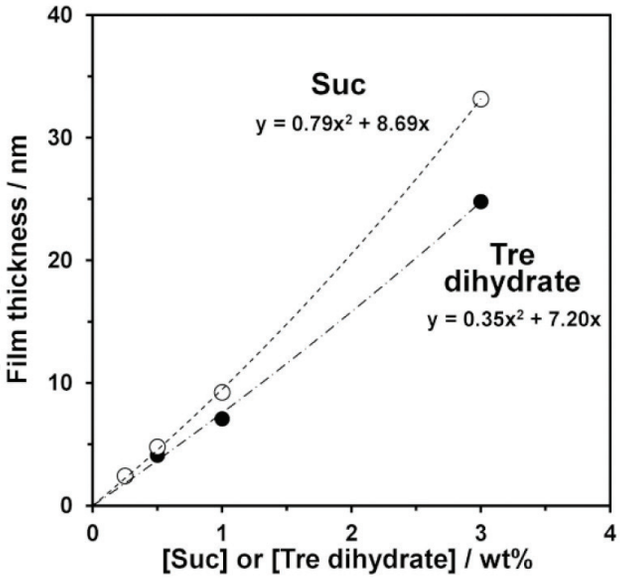

Figure 5. Thicknesses of sugar spun-films versus concentration of the corresponding aqueous sugar solutions used for spin coating. Open and closed circles denote the Suc and Tre sugar forms, respectively.

the higher the concentration of aqueous solution, the thicker the spin-coated film. The film thicknesses as functions of aqueous solution concentration are plotted in **Figure 5**. Each plot is well approximated by a quadratic equation.

3.2. Variation of film thickness of spun-films under reduced pressure

Water traces in the sugar matrix must be considered in studies of amorphous sugar. To confirm the existence of water, we analyzed the thicknesses of the Suc and Tre films in air and vacuum at room temperature and compared the pre-vacuum XRR profiles with those of the post-vacuum and subsequent vacuum release operations. **Figure 6** shows the XRR profiles analyzed (1) before and (2, 3) after the vacuum, together with the profiles (4) after vacuum release. From these results, we recognized that the vacuum operation increased ΔP from 1 to 2 and 3, indicating that the film thickness decreased after the vacuum operation was started. On the other hand, the vacuum release did not discernibly alter the thickness from the pre-release thickness, suggesting that the film thickness was reduced in the vacuum by water evaporation rather than the volume shrinkage of sugar molecules. To deny the hypothesis that the film thickness changed during a phase transition from amorphous to crystalline state, we analyzed the sugar nano-film by specular XRD and non-specular GI-XD. **Figure 7** compares the spectra of the films with those of the commercial powders of Suc and Tre dihydrate crystals. No diffraction peaks assignable to the crystalline structures were identified in the thin-film spectra, supporting that the sugar film did not crystallize during the experiment. Moreover, the XRR analysis detected the water desorption process in the sugar nano-films. After the vacuum operation, the thickness of the Suc spun-film (*ca.* 33.16 nm) had decreased by 5.45 nm, suggesting that water occupied 16.4 vol% in the sugar matrix (**Figure 6a**). In the Tre film of thickness *ca.* 24.7 nm, the vacuum operation removed a water content of approximately 4.4% (**Figure 6b**).

http://dx.doi.org/10.5772/66432

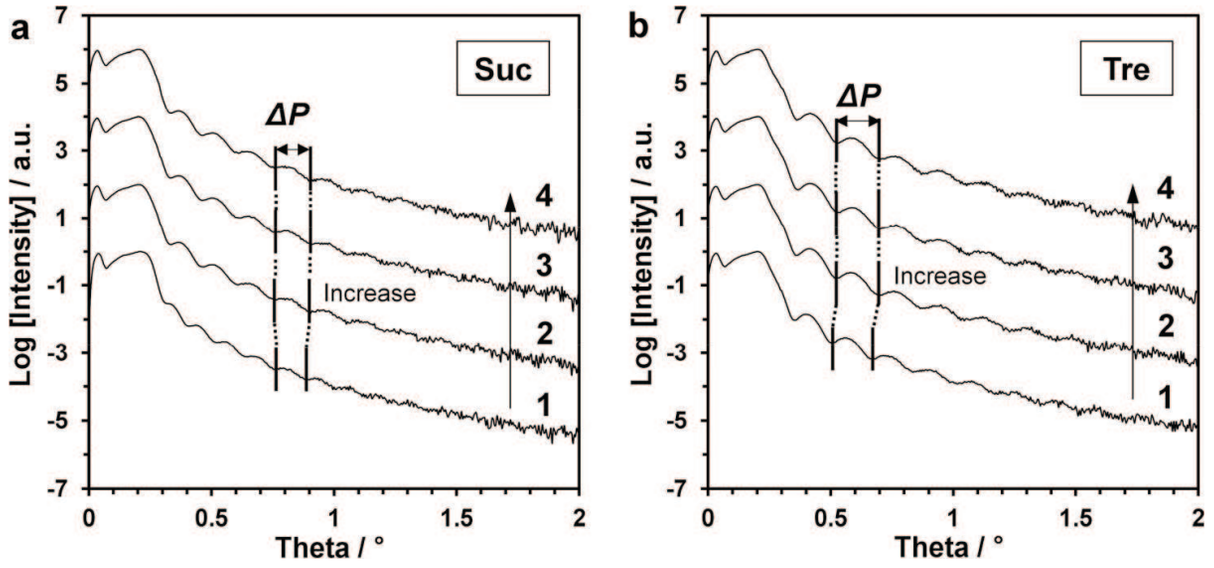

Figure 6. XRR profiles of sugar nano-films (1) before and (2, 3) after vacuum and (4) after vacuum release. Profiles 2 and 3 were obtained after vacuum operation for 15 min and 45 min, respectively. Profiles (1)–(4) represent Suc films with thicknesses of *ca.* 33.16, 27.86, 27.71, and 27.89 nm, respectively (a), and Tre films with thicknesses of *ca.* 24.79, 23.69, 23.45, and 23.52 nm, respectively (b).

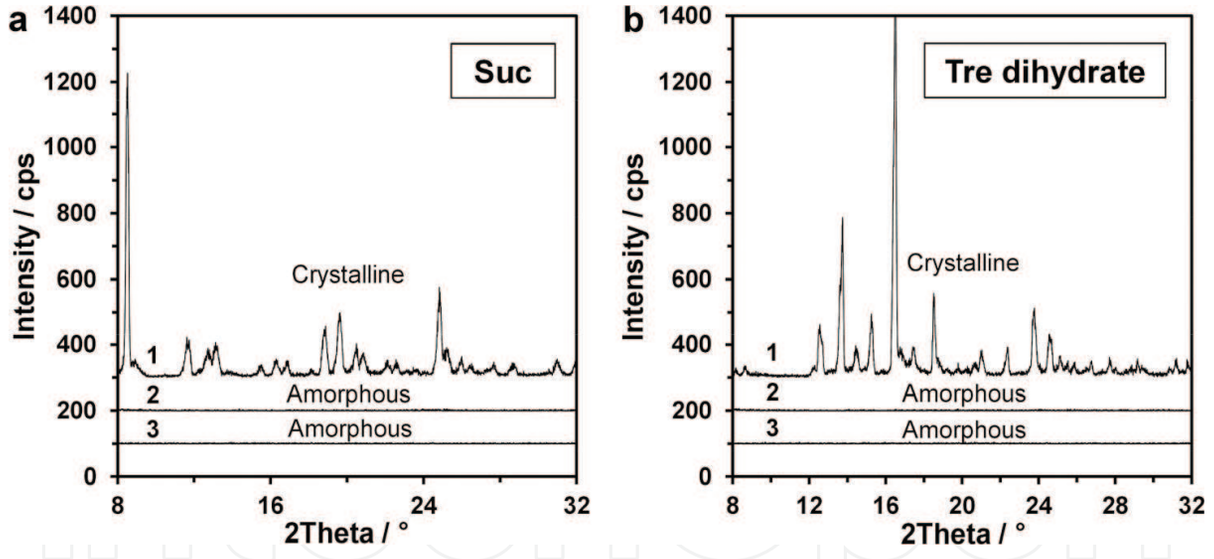

Figure 7. XRD profiles of (1) powder and (2) sugar nano-film and (3) GI-XRD profiles of sugar nano-films. The measured thicknesses of the Suc (a) and Tre (b) films were *ca.* 28 nm and 24 nm, respectively.

3.3. Variation of film thickness with temperature

3.3.1. Temperature-dependent behaviors of sugar nano-films

We next investigated the thickness of sugar nano-films fabricated at different temperatures. Experiments were conducted on Suc and Tre films with initial thicknesses of *ca.* 7.97 and 7.51 nm, respectively (**Figure 8**). Films of both sugars became thinner at higher temperatures (1 in **Figure 8**). The thicknesses of the Suc and Tre films decreased to *ca.* 7.84 nm at 90°C (−1.63%)

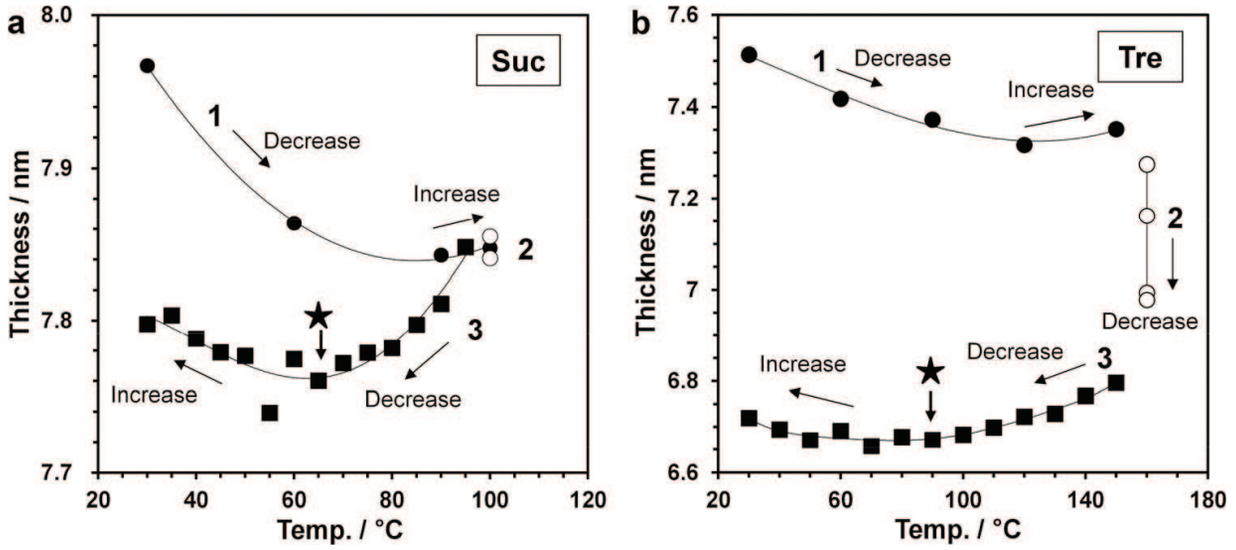

Figure 8. Temperature-dependent thickness changes in Suc and Tre films under vacuum conditions. Initially, the Suc (a) and Tre (b) films were *ca.* 8.0 nm and 7.5 nm thick, respectively. The Suc film was (1) heated from 30°C to 100°C, (2) held at 100°C for 80 min and then (3) cooled to 30°C. The Tre film was (1) heated from 30°C to 160°C, (2) held at 100°C for 150 min, and then (3) cooled to 30°C. The samples were heated and cooled at 5.0°C/min. The measurement time of each plot was 30 min.

and to *ca.* 7.32 nm at 120°C (−2.53%), respectively. No further decrease was observed after subsequent heating to 100°C for Suc film and to 160°C for Tre film (1 in **Figure 8**). Isothermal annealing at 100°C for 80 min did not alter the thickness of Suc film (2 of Suc in **Figure 8**), but isothermal annealing at 160°C reduced the thickness of the Tre film in a time-dependent manner (2 of Tre in **Figure 8**); this problem will be discussed in Section 3.3.3. Despite the different thickness responses of the sugar films at the isothermal annealing stage, the thicknesses of both sugars exhibited similar temperature-dependent behaviors during subsequent cooling (3 in **Figure 8**). Specifically, the film thicknesses decreased with cooling to a certain temperature and then increased with further cooling. The temperature at which the thickness stabilized (indicated by the filled star in the figure) was approximately 70°C for Suc film and 95°C for Tre film. As is well known, the volumes of conventional materials shrink with lowering temperature and its accompanying entropy decrease, but certain materials expand as the temperature reduces. The latter phenomenon, called negative thermal expansion (NTE) [17, 31], was apparently exhibited by the sugar nano-films during the cooling process.

The thermal expansion behavior of the Tre film depended on its thermal history (conditions are described in the caption of **Figure 9**). Similarly to **Figure 8**, the film thickness both decreased and increased during heating process (1 in **Figure 9**), and apparently decreased during isothermal annealing at 150°C (2 in **Figure 9a**). However, during subsequent cooling from 160° to 30°C, no NTE phenomenon was observed (3 in **Figure 9a**). In **Figure 9b** (Case II) the slopes of the normalized thickness versus temperature lines differ between above and below *ca.* 95°C. This temperature-dependent thickness behavior is probably attributable to the glass transition upon cooling. The glassy-to-viscous state transition of T_g is typically determined as the intersection of the two straight lines showing different linear expansivities [18]. In this way, we determined the T_g of trehalose nano-film as 95°C. We also compared the

http://dx.doi.org/10.5772/66432

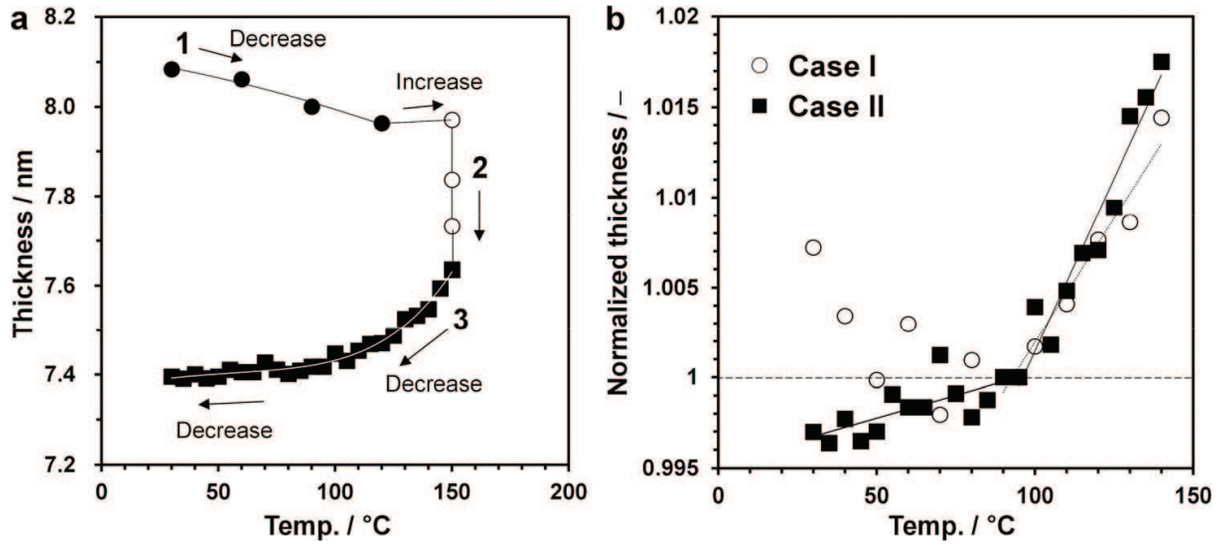

Figure 9. Temperature-dependent thickness changes in Tre film under vacuum conditions with different thermal history from that of **Figure 8b** (a). Initially, the Tre film was *ca.* 8.08 nm thick. The film was (1) heated from 30°C to 150°C, then (2) held at 150°C for 120 min, and (3) cooled to 30°C. The sample was heated and cooled at 10.0°C/min. Comparison of the thickness-temperature profiles in Cases I and II (b). Normalized thicknesses in Cases I and II result from the first cooling in **Figure 8b** and the first cooling in **Figure 9a**, respectively. Each film thickness was normalized by the film thickness at 90°C.

temperature-dependent thickness behaviors of Case I (after isothermal annealing at 160°C for 150 min) and Case II (after isothermal annealing at 150°C for 120 min). Notably, the slopes of the normalized thickness versus temperature lines were comparable above 95°C, despite the different thickness behaviors of Cases I and II below this temperature. From this result, the temperature indicated by the filled star in **Figure 8** was assumed as T_g. Above this temperature, the molecules can rapidly rearrange in the melt state, whereas below this temperature, their molecular mobility must be highly restricted.

3.3.2. Observation of reproducibility of NTE during heating and cooling cycle

NTE has received much attention as a tuning phenomenon in the overall thermal expansion of materials [31]. It has also been observed in ultrathin polymer films [16, 17, 20]. Mukherjee et al. reported NTE below the T_g in polystyrene (PS) films with thicknesses of several dozen nanometers, together with zero thermal expansion (ZTE) behavior [17]. They observed NTE and ZTE during both heating and cooling processes. To confirm the reproducibility of the NTE in the present study, we performed a reheating (second heating) operation. The thickness of the Tre film during reheating from 30°C to 140°C is depicted in **Figure 10a**. Although the second heating yielded slight deviations from the first cooling, the NTE behaviors were consistent in both processes, namely, the thickness decreased up to approximately 95°C and then increased with increasing temperature in the second heating process. Here, we estimated the area density of the electrons (average number of electrons per unit area of film) from the XRR profile and multiplied it by the film thickness. The results are plotted against temperature in **Figure 10b**. During the first cooling and second heating processes, the values were dispersed around the average value without large deviation, indicating that the NTE behavior does not

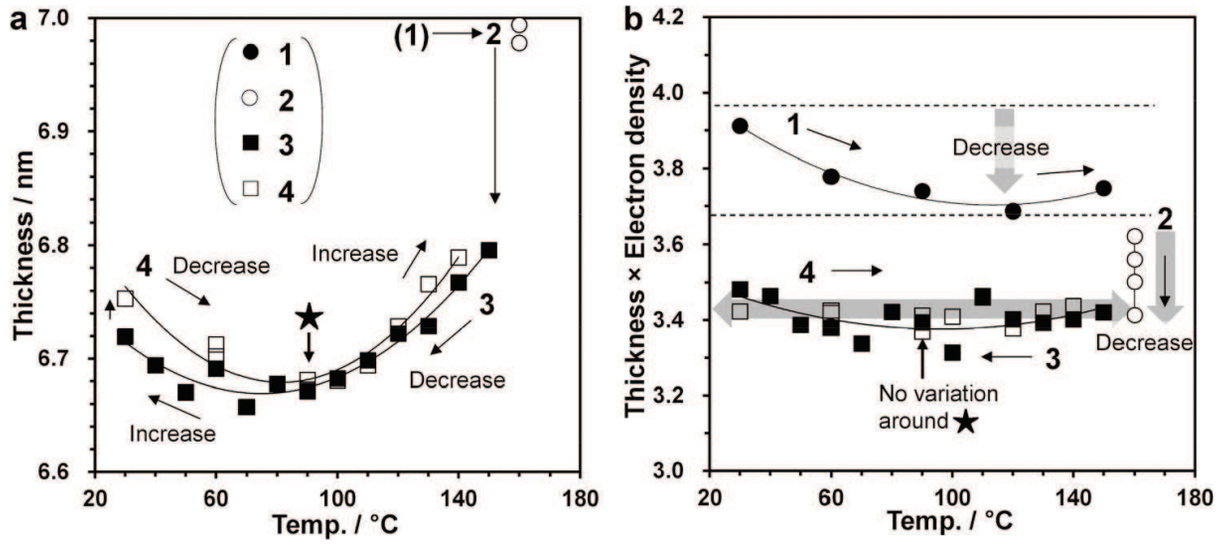

Figure 10. Thickness changes in Tre film during (3) the first cooling and (4) the second heating process (a) and the product of thickness and electron density during (1) the first heating, (2) isothermal annealing, (3) first cooling, and (4) second heating cycles (b). The heating and cooling were carried out at 5.0°C/min.

result from the absorption or desorption of trace amounts of water. Also, the temperature-dependent variation in film thickness was confirmed to occur perpendicularly to the substrate, indicating that the density of the sugar matrix varies with temperature because the film thickness varies with temperature. The film thickness should therefore increase with decreasing density.

In **Figures 7–9**, an apparent hysteresis appears between the thicknesses during the first heating and first cooling and during the first and second heating processes. During the first heating process, the thickness (and its product with the electron density) monotonically decreases with increasing temperature up to 90°C and 120°C for Suc and Tre film, respectively. This effect might be attributable to the evaporation of trace amounts of water during the heating. The filling of the voids left by the departing water molecules might shrink the sugar matrix. Above 90°C for Suc film and 120°C for Tre film, the thickness and electron density product became invariant, suggesting that the water had wholly evaporated. Thus, NTE was observed during the first heating process, but apparently the first cooling process was governed by different mechanisms.

3.3.3. Sublimation problem

The dominant factor governing the inclusion or exclusion of NTE is unclear, but a likely scenario is rearrangement of the sugar matrix in the melt state, as the isothermal conditions are different in Cases I and II. In fact, the largely reduced thickness of the Tre film after isothermal annealing at 160°C was unexpected (see process 2 in **Figure 8b**). The product of thickness and electron density in Tre film exhibited a similar trend (2 in **Figure 10b**). **Figure 11** plots the time-dependent thickness of the Tre film under isothermal annealing at 170°C. Prior to annealing, the film was gradually heated to 150°C. During the heating process, the decrease and subsequent increase in thickness mimicked that of stage (1) in **Figure 8** (**Figure 11b**). In

http://dx.doi.org/10.5772/66432

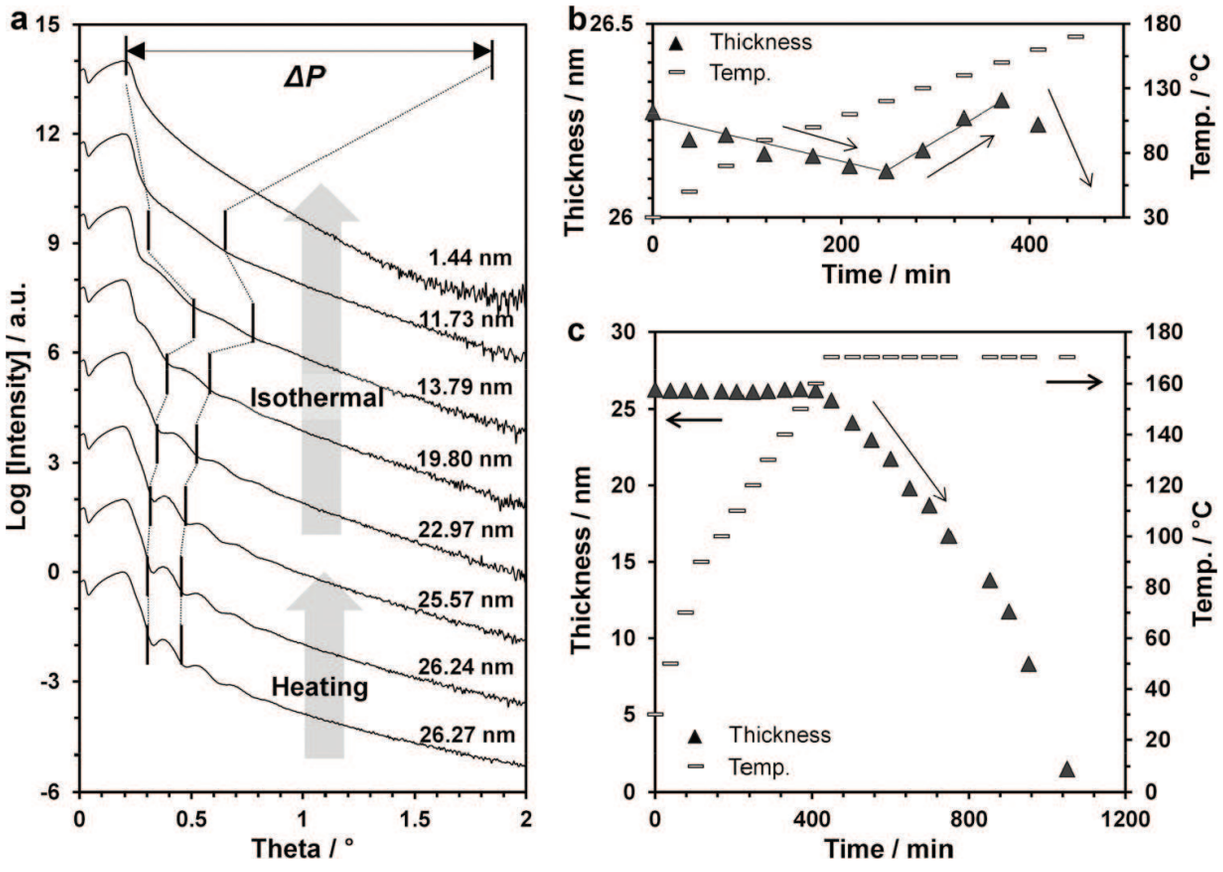

Figure 11. XRR profiles (a) and changing thickness of Tre film under the vacuum condition during heating up to 160°C (b) and during isothermal annealing at 170°C (c).

addition, the thickness began decreasing at 160°C. Subsequently, under isothermal annealing at 170°C, the film thickness continuously decreased, reaching 0 after *ca.* 10 h (**Figure 11c**), as clearly evidenced by the broadening of ΔP in the XRR profiles (**Figure 11a**). This result strongly supports sublimation of the Tre film under high-temperature low-pressure conditions. Because Tre is a small molecule with a molecular weight of 342.3, it can potentially sublimate under these conditions. During sublimation, the molecules at the air-sugar interface are easily rearranged, which would largely influence the whole range of nano-films. Therefore, the isothermal annealing conditions can affect the states of the nano-films and determine the occurrence or absence of NTE. For a more detailed discussion, we should accurately tune the reduced pressure condition to control or prevent the sugar sublimation.

4. Conclusions

In this chapter, we demonstrated the temperature-dependent thickness behaviors of sugar nano-films formed on Si(100) substrates of area (2 × 2) cm^2. Homogeneous flat films suitable for precise XRR analysis were fabricated by the conventional spin-coating method. The complex behaviors of the shrinking and expanding sugar nano-films during heating and cooling were successfully observed and are schematically summarized in **Figure 12**.

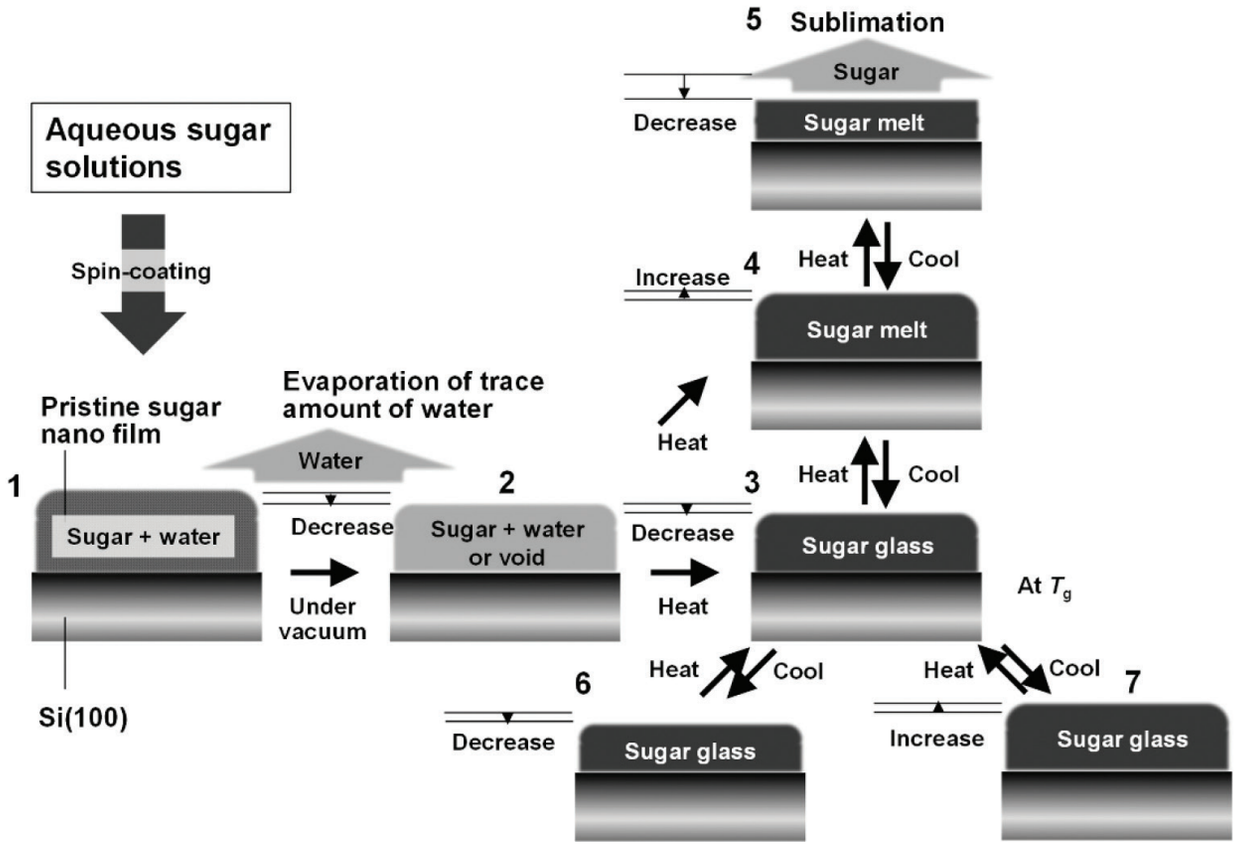

Figure 12. Schematic representation of the behavior of sugar nano-films under reduced pressure.

Once the aqueous sugar solutions have been spin-coated on the Si substrates, residual water remains in the nano-films (1 in **Figure 12**). Such water can be mostly or partly removed by evaporation under reduced pressure even at room temperature (1–2 in **Figure 12**). Evaporation manifests as decreased film thickness. As the T_gs of Suc and Tre are much higher than room temperature, an anhydrous sugar matrix system must exist in the glassy state at room temperature. Otherwise, the system is a sugar matrix adsorbing trace amounts of water. The film thickness was generally decreased by heating operations (2–3 or 4 or the intermediate state of 3 and 4 in **Figure 12**). This decrease is ascribed to the evaporation of remaining water in the sugar matrix. The evaporated water leaves voids that are then filled by contraction of the sugar matrix during the subsequent glass formation. The glassification must prevent the short-time rearrangement of molecules at temperatures below T_g, but as the sugar molecules gain thermal energy when heated above T_g, they can readily rearrange in the matrix. However, under reduced pressure, the relatively low-molecular-weight natural sugars inevitably sublimate, as they lack a nonvolatile property (5 in **Figure 12**). This situation never arises in polymeric film. Beside sublimating themselves in the matrix, the sugar molecules redistribute at the vacuum-sugar interface, which should significantly affect the overall nano-film locating around the interface. As the temperature decreases, sublimation becomes less important, and the thickness might decrease through shrinkage of the sugar matrix under thermodynamic processes. Below T_g, the sugar films showed two behaviors, a normal reduction in film thickness with smaller expansibilities than obtained

between 3 and 4 in **Figure 12** (3–6 in **Figure 12**) and an unusual increase in film thickness governed by NTE (from 3 to 7 in **Figure 12**). These processes appear not to be determined by the initial film thickness; rather, they depend on the thermal history, for reasons which are currently unknown. To understand the effect of molecular rearrangement at the vacuum-sugar interface, we should study anhydrous sugar nano-films under precisely defined vacuum conditions.

As shown in this chapter, the XRR methodology provides profound insights into the adsorption and desorption properties of amorphous sugars, the rearrangement of sugar molecules at the sugar-air interface and the glass transition. To acquire these insights, we observed how the film thickness depends on water content and temperature. By understanding the sugar-vacuum or sugar-solid interface, we might also capture the structural changes of sugar matrixes under freezing, freeze-drying, and spray-drying operations. In all of these processes, molecular transfer such as water adsorption and desorption starts at the interface.

Acknowledgement

This work was financially supported by the Amano Institute of Technology, AIST, Japan, by the MEXT-Supported Program for the Strategic Research Foundation at Private Universities (S1201027) 2012–2016, and by the Japan Society for the Promotion of Science (Grant-in-Aid for Scientific Research (C) 24560033).

Author details

Shigesaburo Ogawa[1] and Isao Takahashi[2]*

*Address all correspondence to: suikyo@kwansei.ac.jp

1 Department of Materials and Life Science, Faculty of Science and Technology, Seikei University, Japan

2 Department of Physics, School of Science and Technology, Kwansei Gakuin University, Japan

References

[1] Kauzmann W: The nature of the glassy state and the behavior of liquids at low temperatures. Chemical Reviews. 1948;43:219–256. DOI: 10.1021/cr60135a002

[2] MacKenzie AP: Non-equilibrium freezing behavior of aqueous systems. Philosophical Transactions of the Royal Society B: Biological Sciences. 1977;278:167–189. DOI: 10.1098/rstb.1977.0036

[3] Slade L, Levine H: Non-equilibrium behavior of small carbohydrate-water systems. Pure and Applied Chemistry. 1988;60:1841–1864. DOI: 10.1351/pac198860121841

[4] Carpenter JF, Crowe LM, Crowe JH: Stabilization of phosphofructokinase with sugars during freeze-drying: characterization of enhanced protection in the presence of divalent cations. Biochimica et Biophysica Acta. 1987;923:109–115. DOI: 10.1016/0304-4165(87)90133-4

[5] Slade L, Levine H, Reid DS: Beyond water activity: recent advances based on an alternative approach to the assessment of food quality and safety. Critical Reviews in Food Science & Nutrition. 1991;30:115–360. DOI: 10.1007/978-1-4899-0664-9_3

[6] Fox KC: Biopreservation. Putting proteins under glass. Science. 1995;267:1922–1923. DOI: 10.1126/science.7701317

[7] Dave H, Gao F, Lee JH, Liberatore M, Ho CC, Co CC: Self-assembly in sugar–oil complex glasses. Nature Materials. 2007;6:287–290. DOI: 10.1038/nmat1864

[8] Santivarangkna C, Higl B, Foerst P: Protection mechanisms of sugars during different stages of preparation process of dried lactic acid starter cultures. Food Microbiology. 2008;25:429–441. DOI: 10.1016/j.fm.2007.12.004

[9] Giri J, Li W-J, Tuan RS, Cicerone MT: Stabilization of proteins by nanoencapsulation in sugar-glass for tissue engineering and drug delivery applications. Advanced Materials. 2011;23;4861–4867. DOI: 10.1002/adma.201102267

[10] Mittal A, Schulze K, Ebensen T, Weissmann S, Hansen S, Guzmán CA, Lehr CM: Inverse micellar sugar glass (IMSG) nanoparticles for transfollicular vaccination. Journal of Controlled Release. 2015;206:140–152. DOI: 10.1016/j.jconrel.2015.03.017

[11] Simatos D, Blond G, Roudaut G, Champion D, Perez J, Faivre AL: Influence of heating and cooling rates on the glass transition temperature and the fragility parameter of sorbitol and fructose as measured by DSC. Journal of Thermal Analysis. 1996;47:1419–1436. DOI: 10.1007/BF01992837

[12] Angell CA: Liquid fragility and the glass transition in water and aqueous solutions. Chemical Reviews. 2002;102:2627–2650. DOI: 10.1021/cr000689q

[13] Surana R, Pyne A, Suryanarayanan R: Effect of preparation method on physical properties of amorphous trehalose. Pharmaceutical Research. 2004;21:1167–1176.

[14] Surana R, Pyne A, Suryanarayanan R: Effect of aging on the physical properties of amorphous trehalose. Pharmaceutical Research. 2004;21:867–874. DOI: 10.1023/B:PHAM.0000026441.77567.75

[15] Saxena A, Jean YC, Suryanarayanan R: Annealing effect reversal by water sorption–desorption and heating above the glass transition temperature-comparison of properties. Molecular Pharmaceutics. 2013;10:3005–3012. DOI: 10.1021/mp400099r

[16] Orts WJ, van Zanten JH, Wu W-L, Satija SK: Observation of temperature dependent thickness in ultrathin polystyrene films on silicon. Physical Review Letters. 1993; 71:867–870. DOI: http://dx.doi.org/10.1103/PhysRevLett.71.86

[17] Mukherjee M, Bhattacharya M, Sanyal MK, Geue T, Grenzer J, Pietsch U: Reversible negative thermal expansion of polymer films. Physical Review E. 2002;66:061801. DOI: 10.1103/PhysRevE.66.061801

[18] Takahashi I, Yang C: Broadening, no broadening and narrowing of glass transition of supported polystyrene ultrathin films emerging under ultraslow temperature variations. Polymer Journal. 2011;43:390–397. DOI: 10.1038/pj.2010.145

[19] Sun X, Guo L, Sato H, Ozaki Y, Yan S, Takahashi I: A study on the crystallization behavior of poly(β-hydroxybutyrate) thin films on Si wafers. Polymer. 2011;52:3865–3870. DOI: http://dx.doi.org/10.1016/j.polymer.2011.06.024

[20] Gin P, Jiang N, Liang C, Taniguchi T, Akgun B, Satija SK, Endoh MK, Koga T: Revealed architectures of adsorbed polymer chains at solid-polymer melt interfaces. Physical Review Letters. 2012;109:265501. DOI: 10.1103/PhysRevLett.109.265501

[21] Tolan M: Springer Tracts in Modern Physics. X-ray Scattering from Soft-Matter Thin Films. Materials Science and Basic Research. Springer: Berlin, vol. 148; 1999. 197 p. DOI: 10.1007/BFb0112834

[22] Yasaka M: X-ray thin-film measurement techniques V. X-ray reflectivity measurement. The Rigaku Journal. 2010;26:1–9.

[23] Kiessig H: Investigation to the total X-ray reflection. Annalen der Physik. 1931;10:715–768. DOI: 10.1002/andp.19314020607

[24] Wright WW, Guffanti GT, Vanderkooi JM. Proteins in sugar films and in glycerol/water as examined by infrared spectroscopy and by the fluorescence and phosphorescence of tryptophan. Biophysical Journal. 2003;85:1980–1995. DOI: http://dx.doi.org/10.1016/S0006-3495(03)74626-8

[25] Cheng J, Wingrad N: Depth profiling of peptide films with TOF-SIMS and a C60 probe. Analytical Chemistry. 2005;77:3651–3659. DOI: 10.1021/ac048131w

[26] Zhu Z, Nachimuthu P, Lea AS: Molecular depth profiling of sucrose films: a comparative study of C_{60}^{n+} ions and traditional Cs^+ and O_2^+ ions. Analytical Chemistry. 2009;81:8272–8279. DOI: 10.1021/ac900553z

[27] He X, Fowler A, Menze M, Hand S, Toner M: Desiccation kinetics and biothermodynamics of glass forming trehalose solutions in thin films. Annals of Biomedical Engineering. 2008;36:1428–1439. DOI: 10.1007/s10439-008-9518-8

[28] Predoi D: Physico-chemical studies of sucrose thin films. Digest Journal of Nanomaterials and Biostructures. 2010;5:373–377.

[29] Zhao B, Zeng H, Tian Y, Israelachvili J: Adhesion and detachment mechanisms of sugar surfaces from the solid (glassy) to liquid (viscous) states. Proceedings of the National Academy of Sciences. 2006;103:19624–19629. DOI: 10.1073/pnas.060952910

[30] Parratt LG: Surface studies of solids by total reflection of X-rays. Physical Review. 1954;95:359–369. DOI: http://dx.doi.org/10.1103/PhysRev.95.359

[31] Takenaka K: Negative thermal expansion materials: technological key for control of thermal expansion. Scientific and Technology of Advanced Materials. 2012;13:013001. DOI: 10.1088/1468-6996/13/1/013001

IntechOpen